AD-A075 474 COLD REGIONS RESEARCH AND ENGINEERING LAB HANOVER NH F/G 8/12
A VOLUMETRIC CONSTITUTIVE LAW FOR SNOW SUBJECTED TO LARGE STRAI--ETC(U)
AUG 79 R L BROWN

UNCLASSIFIED CRREL-79-20 NL

| OF |
AD
A075474

END
DATE
FILMED
11-79
DDC

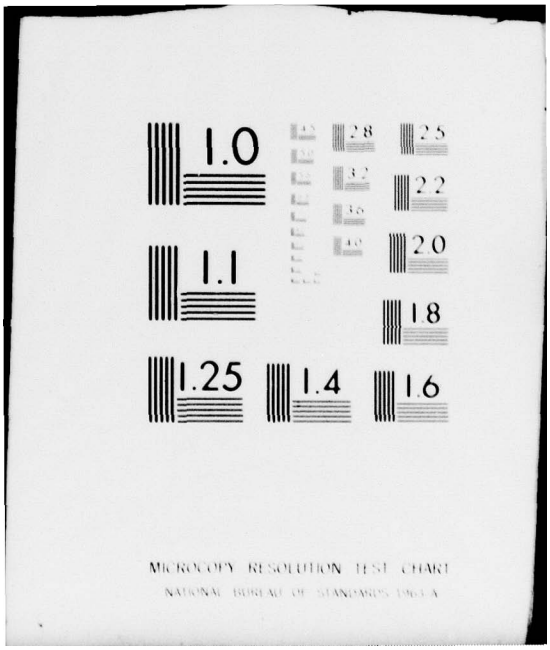
1.0
1.1
1.25
1.4
1.6
2.8
2.5
3.2
2.2
3.6
2.0
4.0
1.8
MICROCOPY RESOLUTION TEST CHART
NATIONAL BUREAU OF STANDARDS 1963-A

CRREL
REPORT 79-20

12

LEVEL II

A volumetric constitutive law for snow subjected to large strains and strain rates

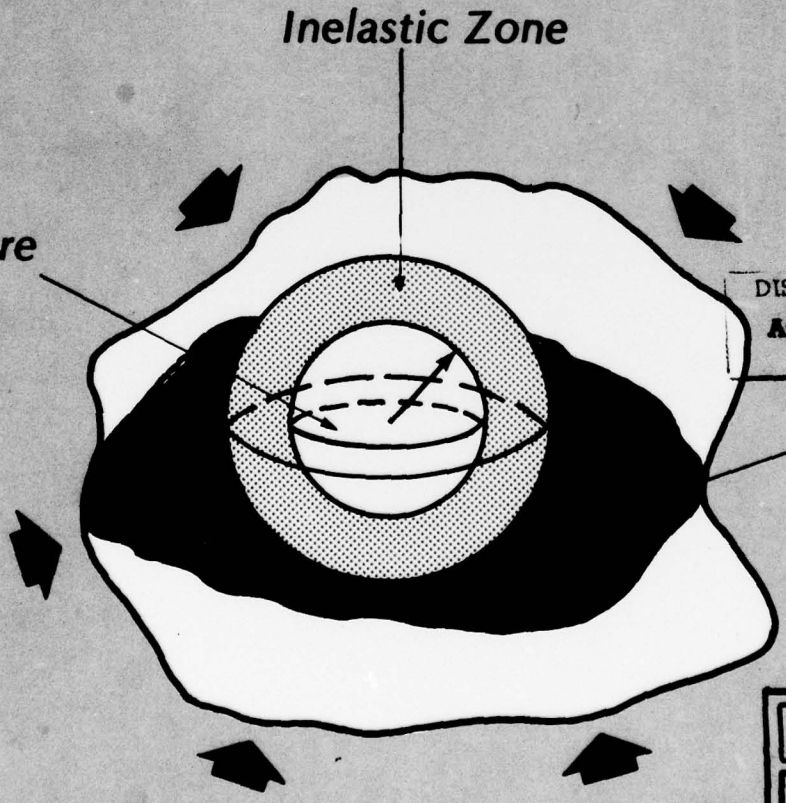

79 10 25 036

Cover: *Pore collapse model used to develop the volumetric constitutive law for snow. Both elastic and inelastic deformation regions are illustrated.*

(14)
CRREL Report 79-20

(6)
A volumetric constitutive law for snow subjected to large strains and strain rates

(10)
Robert L. Brown

(12) 20

(16) 4A161102AT24

(11)
August 1979

(17) A1

Prepared for
DIRECTORATE OF MILITARY PROGRAMS
OFFICE, CHIEF OF ENGINEERS
By
UNITED STATES ARMY
CORPS OF ENGINEERS
COLD REGIONS RESEARCH AND ENGINEERING LABORATORY
HANOVER, NEW HAMPSHIRE, U.S.A.

037100

46

REPORT DOCUMENTATION PAGE

READ INSTRUCTIONS BEFORE COMPLETING FORM

1. REPORT NUMBER: CRREL-Report 79-20	2. GOVT ACCESSION NO.
3. RECIPIENT'S CATALOG NUMBER	
4. TITLE (and Subtitle): A VOLUMETRIC CONSTITUTIVE LAW FOR SNOW SUBJECTED TO LARGE STRAINS AND STRAIN RATES	5. TYPE OF REPORT & PERIOD COVERED
	6. PERFORMING ORG. REPORT NUMBER
7. AUTHOR(s): Robert L. Brown	8. CONTRACT OR GRANT NUMBER(s): U.S. Army Research Grant DRXRO-GS-15413
9. PERFORMING ORGANIZATION NAME AND ADDRESS: U.S. Army Cold Regions Research and Engineering Laboratory, Hanover, New Hampshire 03755	10. PROGRAM ELEMENT, PROJECT, TASK AREA & WORK UNIT NUMBERS: DA Project 4A161102AT24, Task A1, Work Unit 001
11. CONTROLLING OFFICE NAME AND ADDRESS: Directorate of Military Programs, Office, Chief of Engineers, Washington, D.C. 20314	12. REPORT DATE: August 1979
	13. NUMBER OF PAGES: 18
14. MONITORING AGENCY NAME & ADDRESS (if different from Controlling Office)	15. SECURITY CLASS. (of this report): Unclassified
	15a. DECLASSIFICATION/DOWNGRADING SCHEDULE

16. DISTRIBUTION STATEMENT (of this Report)

Approved for public release; distribution unlimited.

17. DISTRIBUTION STATEMENT (of the abstract entered in Block 20, if different from Report)

18. SUPPLEMENTARY NOTES

19. KEY WORDS (Continue on reverse side if necessary and identify by block number)

Compression
Constitutive law
Deformation
Snow
Viscoplasticity
Volumetric properties

20. ABSTRACT (Continue on reverse side if necessary and identify by block number)

A volumetric constitutive equation was developed to characterize the behavior of snow subjected to large compressive volumetric deformations. By treating the material as a suspension of air voids in a matrix material of polycrystalline ice, a rate-dependent volumetric constitutive law was formulated and found to accurately predict material response to pressure loads for a wide range of load rates. The apparent valid range for strain rates was 10^{-5} s^{-1} to 10 s^{-1}, and the equation appeared to work well for initial densities above 300 kg m^{-3}.) Comparison of the theory with shock wave data was not considered in this paper, although the constitutive law appears to be valid for such load situations. One application to oversnow mobility of tracked vehicles was made. In this case, power requirements due to snow compaction were calculated parametrically in terms of vehicle speed, track loading, and snow density.

PREFACE

This report was prepared by Robert L. Brown, Visiting Scientist, Snow and Ice Branch, Research Division, U.S. Army Cold Regions Research and Engineering Laboratory, on sabbatical leave from Montana State University, Bozeman, Montana.

This study was funded primarily under U.S. Army Research Grant No. DRXRO-GS-15413 to Montana State University. The study was also funded under DA Project 4A161102AT24, *Research in Snow, Ice and Frozen Ground*; Task A1, *Properties of Cold Regions Materials*; Work Unit 001, *Properties of Snow and Ice.*

Technical review of this report was performed by Dr. M. McPhee and R. Berger of CRREL.

The author expresses appreciation to the Army Research Office and the U.S. Army Cold Regions Research and Engineering Laboratory for their support.

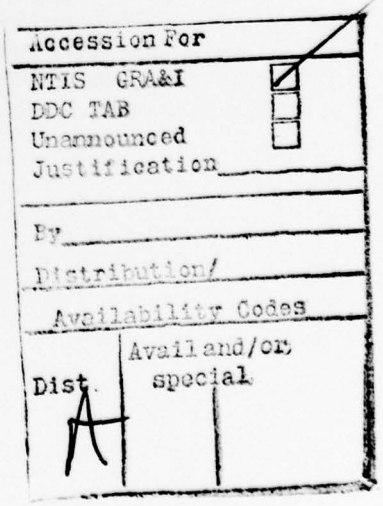

CONTENTS

ILLUSTRATIONS

NOMENCLATURE

a, b	internal and external radii (m)
c	elastic-viscous interface radius (m)
e	deviatoric strain
h	height of test specimen
p	hydrostatic pressure porous material (bar)
r	radial coordinate (m)
u	radial displacement (m)
v	velocity (m s^{-1})
x_1, x_2, x_3	deformed coordinate positions
A, C, ϕ, S_0, J	material constants
B, k, F	time functions
D	principal difference value of deformation rate tensor (s^{-1})
$\underset{\sim}{D}$	rate of deformation tensor (s^{-1})
$\underset{\sim}{F}$	undetermined time function
G	shear modulus (bar)
$H(t)$	Heaviside step function
P	external pressure (bar)
P^*	nominal track pressure
S	principal difference value of stress tensor
$\underset{\sim}{S}$	deviatoric stress tensor
$\underset{\sim}{T}$	Cauchy stress tensor (bar)
V	volume (m^3)
$\dot{W}$	stress power
X_1, X_2, X_3	undeformed coordinate positions
Y	yield stress (bar)
α	density ratio
$\dot{\alpha}$	rate of change of density ratio
$\dot{\gamma}$	shear strain rate (s^{-1})
ϵ	strain
$\dot{\epsilon}$	strain rate (s^{-1})
ρ	mass density (Mg m^{-3})
σ	stress (bar)
τ	shear stress
ϕ, θ	spherical coordinate angles (rad)
Ψ	acceleration potential (m^2 s^{-2})

Subscripts

a	inner radial position
b	outer radial position
c	interface position
i, j	i-j th components of a tensor
m	matrix material
o	initial value
r	radial coordinate component
1, 2, 3	principal values
ϕ	ϕ coordinate component

CONVERSION FACTORS: U.S. CUSTOMARY TO METRIC (SI) UNITS OF MEASUREMENT

These conversion factors include all the significant digits given in the conversion tables in the ASTM *Metric Practice Guide* (E 380), which has been approved for use by the Department of Defense. Converted values should be rounded to have the same precision as the original (see E 380).

Multiply	*By*	*To obtain*
inch	25.4*	millimeter
foot	0.3048*	meter
foot^2	0.09290304*	meter^2
pound-mass	0.4535924	kilogram
pound-force/inch^2	0.0680	bar
gallon	0.003785412	meter^3
degrees Fahrenheit	$t°_C = (t°_F - 32)/1.8$	degrees Celsius

*Exact

A VOLUMETRIC CONSTITUTIVE LAW FOR SNOW SUBJECTED TO LARGE STRAINS AND STRAIN RATES

Robert L. Brown

1. INTRODUCTION

Snow is a granular or porous material comprising an ice-air mixture. Because of its high porosity, it is capable of undergoing large volumetric deformations that are largely irreversible. Since snow is so highly compressible, its density should naturally be expected to be a central property which is used to define other properties such as shear strength and thermal conductivity. Indeed, a close relationship between density and many of the mechanical and physical properties of snow has long been established, although density alone is not an adequate parameter for characterizing the mechanical properties of snow.

Since density (or porosity) is an important parameter, the volumetric properties of snow will be analyzed in this report. In particular, an attempt will be made to develop a volumetric constitutive equation relating material porosity to pressure loading. Special attention will be given to monotonic loads generating strain rates ranging from a low rate (10^{-5} s^{-1}) to rates above 10 s^{-1}.

Snow is idealized as a suspension of air voids or pores in an incompressible elastic-viscoplastic material, and the change in its porosity is characterized in terms of the collapse of these air voids under compressive loading. This is done by considering the compressive loading of a thick-walled hollow sphere of polycrystalline ice. This model, while necessarily a rather simplistic one, does contain the essential features of material porosity and the properties of the matrix material. It also reflects the physical processes which are necessary to produce material flow to reduce pore size, so that the basic form of the resulting constitutive equation should be correct.

Some simplifying assumptions made in the analysis have to be accounted for. In particular, the model used here assumes no interaction between pores, whereas medium-density snow has a high degree of interconnection of pores. This results in a stress intensification in the matrix material and reduces the material stiffness from what the present analysis will indicate. To take these effects into account, a scale factor and a work-hardening term must be added to the derived constitutive law. This will be discussed in more detail later. Carroll and Holt (1972) used a similar approach to analyze successfully the response of porous aluminum to transient loads. In their work, they assumed the material to be an elastic, perfectly plastic material,* whereas in the present study a rate-dependent response of the material must be considered.

This report first considers the constitutive law for ice. Since relatively high strain rates and predominantly compressive states of stress are considered here, a relatively simple form avoiding tensorial arguments is used. The report then considers a detailed development of the constitutive law for snow, followed by an evaluation of the results and a discussion of some applications.

2. MATERIAL REPRESENTATION OF ICE

Previous studies by Dillon and Andersland (1967) and Hawkes and Mellor (1972) have indicated that polycrystalline ice under uniaxial tension and compression possesses a rate-dependent yield stress. Additional experimental work by Haynes (1976) has extended the previous work to strain rates in excess of 1.0 s^{-1}. In tension, ice generally fractures at high strain rates, and this critical stress is not strongly rate

*An elastic, perfectly plastic material behaves as a linear elastic material until a yield condition is reached. Thereafter, under continued loading, the material deforms in a nonhardening manner.

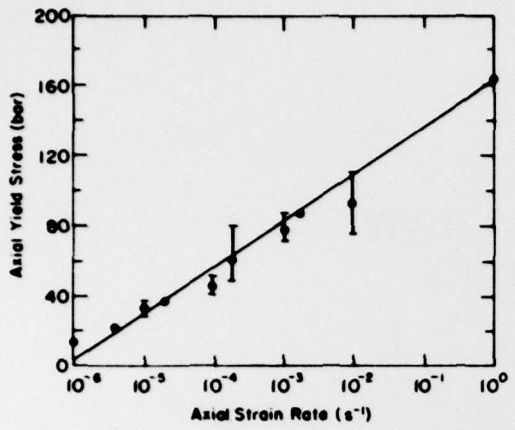

Figure 1. Variation of axial yield stress with axial strain rate for polycrystalline ice [from Dillon and Andersland (1967)].

dependent. However, under compression, the critical stress shows a definite rate dependency, even at the rates studied by Haynes (1976). The present study primarily concerns the compressive properties of ice for intermediate-to-high deformation rates.

Based on the experimental results indicated in Figure 1 (Dillon and Andersland 1967, Haynes 1976), the following constitutive relation is assumed for polycrystalline ice:

$$S = 2Ge \qquad S < Y \tag{2.1}$$

$$S = Y \tag{2.2}$$

where

$$Y = S_0 + C \ln(AD) \qquad AD > 1 \tag{2.3}$$

S_0, C, and A are material constants; S, e, and D are the principal difference values of, respectively, the deviatoric stress tensor, deviatoric strain tensor, and deviatoric deformation rate tensor; and G is shear modulus. For instance, if S_1 and S_3 are the maximum and minimum principal values of the deviatoric stress tensor, then $S = S_1 - S_3$. Similar definitions hold for D and e. The matrix material, ice, is assumed to be incompressible, so that the deviatoric values of the strain tensor and the deformation rate tensors equal the total strain and deformation rate tensors.

The above equations are essentially those of an elastic-viscoplastic material, so that the material behaves elastically until a rate-dependent yield condition is reached, whereupon plastic deformation ensues. These equations are somewhat different from Glen's flow law,

$$\tau = C\dot{\gamma}^n \tag{2.4}$$

where τ and $\dot{\gamma}$ are, respectively, the shear stress and shear strain rate, C is a material constant and n is a scalar. Equations 2.1-2.3 were chosen, since they acquire a straight-line form on Figure 1 and fit the data better than Glen's law. Glen's law does work well at lower strain rates, however, and in many cases is mathematically more tractable than the form of eqs 2.1 - 2.3.

Consider now a compression test on polycrystalline ice. The only nonzero stress component is σ_{xx}, where the x-direction is the axial direction of the compression test. The deviatoric stress tensor is

$$\underset{\sim}{S} = \underset{\sim}{\sigma} - \frac{1}{3}\,(tr\,\underset{\sim}{\sigma})\,\underset{\sim}{1} \tag{2.5}$$

where tr implies the trace of the tensor, $\underset{\sim}{1}$ is the identity tensor, and $\underset{\sim}{\sigma}$ is the Cauchy stress tensor. $\underset{\sim}{S}$ therefore has the components

$$S_{ij} = \begin{bmatrix} \frac{2\sigma_{xx}}{3} & 0 & 0 \\ 0 & -\frac{\sigma_{xx}}{3} & 0 \\ 0 & 0 & -\frac{\sigma_{xx}}{3} \end{bmatrix} \tag{2.6}$$

The rate of deformation tensor is

$$\underset{\sim}{D} = \frac{1}{2}\,(\vec{\nabla}\underline{v} + \underline{v}\overleftarrow{\nabla}) \tag{2.7}$$

where $\vec{\nabla}$ is the gradient operator and $\underline{v}$ is the velocity vector. Since the material is incompressible, the divergence of the velocity field is zero,

$$\vec{\nabla} \cdot \underline{v} = 0 \tag{2.8}$$

and it can be shown that $\underset{\sim}{D}$ has the components

$$D_{ij} = \begin{bmatrix} \frac{\partial v_x}{\partial x} & 0 & 0 \\ 0 & -\frac{1}{2}\frac{\partial v_x}{\partial x} & 0 \\ 0 & 0 & -\frac{1}{2}\frac{\partial v_x}{\partial x} \end{bmatrix} \qquad (2.9)$$

The principal difference values, S and D, are, respectively,

$$S = \sigma_{xx}$$

$$D = \frac{3}{2}\frac{\partial v_x}{\partial x}. \qquad (2.10)$$

In the results reported in Figure 1, strains were all small, so that the axial rate of deformation component D_{xx} is approximately equal to the axial strain rate $\dot{\epsilon}_{xx}$. For uniaxial compression, eq 2.3 becomes

$$\sigma_{xx} = S_0 + C \ln\left(\frac{3A}{2} D_{xx}\right). \qquad (2.11)$$

By adjusting eq 2.11 to fit the compression data represented in Figure 1

$$S_0 = 1 \times 10^6 \text{ N m}^{-2}$$

$$C = 1.165 \times 10^6 \text{ N m}^{-2} \qquad (2.12)$$

$$A = 3.3 \times 10^{+5} \text{s}.$$

As can be seen in Figure 1, this equation represents the test results quite well. There is an appreciable amount of scatter indicated by the vertical lines. This is to be expected, as there may be a good degree of variability in freezing the ice, in forming the specimens, and in testing. However, the average results appear to be well approximated by the constitutive law.

The constitutive law, eqs 2.1-2.3, does not involve a work-hardening term. Previous experimental studies on ice by Dillon and Andersland (1962), among others, have not indicated strong work-hardening* characteristics for ice. However, there are no published data on ice involving large strains in excess of several hundred percent. Therefore, it is quite possible that at large strains ice does exhibit work-hardening properties. Such strains certainly do occur during finite compaction of snow, particularly in the very critical grain bonds where massive localized deformations take place. Thus, the constitutive equation finally formulated for snow may have to be empirically adjusted with a work-hardening term.

This problem has also been encountered in the field of powder metallurgy where a porous metal with an elastic, perfectly plastic matrix material shows considerable work-hardening characteristics. Quite possibly the large strains occurring in high stress regions such as grain bonds are of such an order of magnitude that the matrix material does work harden. Also, quite possibly the actual description of the deformation process is incomplete. At any rate, the work-hardening characteristics of porous materials such as powdered aluminum are not predicted by experiments that have been run on the solid matrix material.

*A work-hardening material is one that stiffens under plastic deformation.

3. DEVELOPMENT OF THE VOLUMETRIC CONSTITUTIVE LAW FOR SNOW

Consider now the deformation of a thick-walled hollow sphere of an incompressible viscoplastic material with the constitutive relation given by eqs 2.1-2.3. The initial internal and external radii of the sphere, a_0 and b_0, are chosen so that the correct material porosity results. In this paper, the density ratio is defined as

$$\alpha = \frac{\rho_m}{\rho} \qquad (3.1)$$

where ρ and ρ_m are, respectively, the mass density of the porous material and the matrix material, ice.

Under an external time-dependent pressure loading, the internal and external radii $a(t)$ and $b(t)$ change with time. The deformation is spherically symmetric, so the deformed coordinates of a generic point can be expressed as:

$$r = r(r_0, t)$$

$$\theta = \theta_0 \qquad (3.2)$$

$$\phi = \phi_0$$

where r_0, θ_0, ϕ_0 are the undeformed spherical coordinate positions, and r, θ, ϕ denote the deformed coordinate positions.

Incompressibility of the matrix material requires the Jacobian of the deformation to equal unity; i.e.,

$$\frac{r^2}{r_0^2}\frac{\partial r}{\partial r_0} = 1. \qquad (3.3)$$

Integration yields

$$r^3 = r_0^3 - B(t) \tag{3.4}$$

where B is an unknown function of time. This equation can be differentiated twice. This results in

$$\ddot{r} = -\left(\frac{2}{9}\frac{\dot{B}^2}{r^5} + \frac{\ddot{B}}{3r^2}\right) \tag{3.5}$$

for the radial acceleration. The acceleration can be expressed in terms of an acceleration potential $\psi(r,t)$:

$$\ddot{r} = \frac{\partial \psi}{\partial r}. \tag{3.6}$$

By doing this, the following can be arrived at for all $a \leq r \leq b$:

$$\psi = \frac{\dot{B}^2}{18r^4} + \frac{\ddot{B}}{3r}. \tag{3.7}$$

The above results are strictly of a kinematical nature and depend only on the constraint of material incompressibility. In addition, material incompressibility may be used to arrive at the following relations:

$$\alpha = \frac{b^3}{(b^3 - a^3)}, \quad \alpha_0 = b_0^3/(b_0^3 - a_0^3) \tag{3.8a}$$

$$a^3 = \frac{a_0^3(\alpha - 1)}{(\alpha_0 - 1)}, \quad b^3 = \frac{a_0^3 \alpha}{(\alpha_0 - 1)} \tag{3.8b}$$

$$B(t) = \frac{a_0^3(\alpha_0 - \alpha)}{(\alpha_0 - 1)}. \tag{3.8c}$$

As the external pressure P increases, the deformation proceeds in three distinct phases:

(1) an initial purely elastic phase,

(2) an elastic-plastic phase with an elastic/plastic interface at $r = c$, where $a \leq c \leq b$, and

(3) a fully plastic phase.

During the first two phases, the strains are assumed to be small, but during the fully plastic phase, large strains can be incurred. Each phase is now considered separately.

Fully elastic phase

In this phase, the strains are assumed to be infinitesimal. Therefore the three strain components are

$$\epsilon_r = \frac{\partial u}{\partial r}, \quad \epsilon_\phi = \epsilon_\theta = u/r \tag{3.9}$$

where u is the radial displacement; and if u is small compared with r, $u = r - r_0$ may be approximated by the expression

$$u = -\frac{B(t)}{3r_0^2}. \tag{3.10}$$

For small strains, r_0 differs by a small amount from r; therefore, in this section the distinction will be dropped. The strains become

$$\epsilon_r = \frac{2}{3}\frac{B}{r^3} \tag{3.11}$$

$$\epsilon_\theta = \epsilon_\phi = -\frac{B}{3r^3}. \tag{3.12}$$

Since the material is assumed to be linearly elastic, the constitutive equation acquires the form

$$S_r = 2Ge_r = 4GB/(3r^3) \tag{3.13a}$$

$$S_\theta = 2Ge_\theta = -2GB/(3r^3) \tag{3.13b}$$

$$S_\phi = 2Ge_\phi = -2GB/(3r^3) \tag{3.13c}$$

where S_r, S_θ, S_ϕ and e_r, e_θ, e_ϕ are, respectively, the deviatoric stress and deviatoric strain components. Since the material is incompressible, the volumetric strain is zero, and the hydrostatic pressure p cannot be evaluated with the constitutive equation alone.

The radial equation of motion is

$$\frac{\partial \sigma_r}{\partial r} + \frac{2}{r}(\sigma_r - \sigma_\phi) = \rho_m \ddot{r} \tag{3.14}$$

which may be put in the modified form

$$-\frac{\partial p}{\partial r} = \rho_m \frac{\partial \psi}{\partial r} \tag{3.15}$$

for which the boundary conditions are:

$$\sigma_r = 0 \qquad r = a \tag{3.16}$$

$$\sigma_r = -P(t) \qquad r = b. \tag{3.17}$$

It should be noted here that pore pressure is assumed negligible. Under extremely large rates of loading or near low density ratios (say $1<\alpha\ll 1.2$), the wisdom of this assumption may be questionable. This will be discussed in more detail later. Integration of eq 3.15 results in:

$$-p\ (r,t) = \rho_m \psi(r,t)+h(t) \tag{3.18}$$

where $h(t)$ is a time function. Since $\sigma_r = S_r - p$,

$$\sigma_r = \rho_m \psi+h+4GB/(3r^3). \tag{3.19}$$

Applying the boundary conditions gives the solution

$$P(t) = \rho_m (\psi_a-\psi_b)+\frac{4GB}{3}\left(\frac{1}{a^2} - \frac{1}{b^2}\right). \tag{3.20}$$

α can then be expressed directly in terms of $P(t)$ by making appropriate use of eqs 3.7 and 3.8. These, combined with eq 3.20, yield

$$P(t) = \tau^2\, Q(\ddot{\alpha}, \dot{\alpha}, \alpha)+\frac{4G(\alpha_0-\alpha)}{3\alpha(\alpha-1)} \tag{3.21}$$

where

$$\tau^2 = \rho_m\, a_0^2/[3\ (\alpha_0-1)^{2/3}]$$

$$Q = -\ddot{\alpha}[\alpha-1)^{-1/3} -\alpha^{-1/3}] \tag{3.22}$$

$$+\frac{1}{6}\dot{\alpha}^2\ [(\alpha-1)^{-4/3} -\alpha^{-4/3}].$$

Equation 3.22 describes the material volumetric response to a hydrostatic pressure loading. The term $P(t)$ represents the actual pressure in the matrix material. Carroll and Holt (1972) have shown that the average pressure in the porous material $\hat{p}(t)$ is approximately

$$\hat{p} = P/\alpha. \tag{3.23}$$

As long as the material does not yield, eq 3.21 describes the time-dependent response of the material. This equation is the same as Carroll and Holt's (1972) result in their study of porous aluminum.

Elastic-plastic phase

Equation 3.19 indicates that the maximum stress occurs at the inner radius. Yielding then initiates there; and, as the pressure $P(t)$ continues to increase, a yield surface, $r = c(t)$, propagates radially outward. The yield condition given by eq 2.3 is reached at a critical pressure P_1 when the principal deviatoric stress difference, S_r-S_θ, reaches the critical value Y, which itself is rate dependent.

Assume now $P \geq P_1$ and that yielding has propagated out to a radial distance c, $a\leq c\leq b$. For $r\leq c$, an inelastic stress state exists, and for $r\geq c$, the material is elastic. When analyzing the outer elastic zone, the following boundary conditions apply:

$$\sigma_r = -P(t),\ r = b \tag{3.24}$$

$$\sigma_r = -P_c(t),\ r = c \tag{3.25}$$

$$S_r-S_\theta = \frac{2GB}{C^3} = Y,\ r = c. \tag{3.26}$$

At the interface of the elastic zone and plastic zone, the stress must satisfy the yield condition. In the yielded zone, eq 2.3 gives

$$S_r = \frac{2}{3}Y = \frac{2}{3}(S_0+C\ 1n\ AD) \tag{3.27}$$

which remains valid as long as the loading is monotonic.

Consider first the yielded zone, where the constitutive law is defined in terms of the deformation rate tensor. The principal rate components are, if v_θ and v_ϕ are zero,

$$D_{rr} = \partial v_r/\partial r \tag{3.28}$$

$$D_{\theta\theta} = v_r/r \tag{3.29}$$

$$D_{\phi\phi} = v_r/r. \tag{3.30}$$

The shearing components are zero. Since the deformation is viscous, a Eulerian description can be used here. Incompressibility requires that the divergence of the velocity vector vanish; i.e.,

$$\frac{\partial v_r}{\partial r} + 2\frac{v_r}{r} = 0$$

or

$$\frac{\partial}{\partial r}(v_r r^2) = 0 \tag{3.31}$$

This yields

$$v_r = \frac{F(t)}{r^2} \tag{3.32}$$

where F is an undetermined time function. Differentiating the above and equating to the acceleration potential results in

$$\psi = -\frac{\dot{F}}{r} + \frac{1}{2}\frac{F^2}{r^4}. \tag{3.33}$$

Actually $F(t)$ can be related directly to $B(t)$ defined in eq 3.7, which can be done by differentiating B to obtain

$$\dot{B}(t) = -3F(t) \tag{3.34}$$

which should be expected, since F and B have been based on the purely kinematical constraint of material incompressibility.

Utilizing the incompressibility constraints in eq 3.8 gives

$$F(t) = \frac{a_0^3 \dot{\alpha}}{3(\alpha_0 - 1)}. \tag{3.35}$$

Now consider the radial equation of motion. In terms of the deviatoric stress components,

$$\frac{\partial S_r}{\partial r} + \frac{2}{r}(S_r - S_\theta) - \frac{\partial p}{\partial r} = \rho_m \frac{\partial \psi}{\partial r}. \tag{3.36}$$

The principal deviatoric deformation rate difference is

$$D = D_{rr} - D_{\theta\theta} = -3F/r^3 \tag{3.37}$$

and the difference $S_r - S_\theta$ can easily be seen to have the value Y. Solution of the equation of motion gives

$$p(t) = \frac{2}{3}S_0 + 2S_0 \ln(r/\beta)$$

$$+C \ln(\beta/r)^3 \left\{\frac{2}{3} + \ln(r/\beta)\right\} - \rho_m \psi + k(t) \tag{3.38}$$

where

$$\beta = \left[-3Ft\right]^{1/3} \tag{3.39}$$

and $k(t)$ is a time integration function resulting from solution of the equation of motion. If we denote as $-P_c$ the value of the radial stress at the interface $r = c$, application of the stress boundary conditions to eq 3.38 gives

$$P_c = 2(S_0 - C)\ln(c/a) + 3C \ln(c/a) \ln\left(\frac{\beta^2}{ca}\right)$$

$$-\rho_m(\psi_c - \psi_a) \tag{3.40}$$

where ψ_a and ψ_c denote the value of ψ at $r = a$ and c, respectively. This must then be equated to the radial stress obtained from the solution of the elastic zone $c \le r \le b$.

In the elastic zone, a procedure identical to that followed in the first phase of the deformation can be followed to arrive at the following solution:

$$P_c = P - \frac{4}{3}GS(c^{-3} - b^{-3}) - \rho_m(\psi_c - \psi_b). \tag{3.41}$$

P_c can be eliminated from eqs 3.40 and 3.41:

$$P(t) = \frac{4}{3}GS(c^{-3} - b^{-3}) - 3\ln\left(\frac{c}{a}\right)\left[2S_0 + 3C\ln\left(\frac{\beta^2}{ca}\right)\right]$$

$$-\rho_m(\psi_a - \psi_b) \tag{3.42}$$

and b and c can subsequently be eliminated by means of eqs 3.36, 3.37, 3.41 and 3.42, so that a relationship between α and P can be established. Since, as will be shown later, this intermediate phase is not of much interest, this final equation will not be developed here.

Fully plastic phase

Once c reaches b, the sphere becomes fully viscous, and the full sphere can be considered with one constitutive equation. The equation of motion, once the appropriate substitutions are made, once again yields eq 3.38, except that this time the boundary conditions given by eqs 3.16 and 3.17 apply. Application of the boundary conditions results in:

$$P(t) = \ln\left[\left(\frac{\alpha}{\alpha-1}\right)^{1/3}\right]\left\{2(S_0-C)+3C\ln\left[\frac{(-\dot{\alpha}A)^{2/3}}{(\alpha(\alpha-1))^{1/3}}\right]\right\}-\rho_m(\psi_b-\psi_a). \quad (3.43)$$

As indicated by eq 3.43, the pressure response of the material consists of two parts: (a) a quasi-static part and (b) a dynamic part as represented by the acceleration potential term $\rho_m(\psi_b-\psi_a)/\alpha$.

The acceleration term can easily be shown to be

$$\rho_m(\psi_b-\psi_a) = \frac{-\rho_m a_0^3}{3(\alpha_0-1)}\left(\frac{1}{b}-\frac{1}{a}\right)\ddot{\alpha} + \frac{\rho_m a_0^6}{18(\alpha_0-1)^2}(b^{-4}-a^{-4})\dot{\alpha}^2 \quad (3.44)$$

where a and b are expressible in terms of α by eq 3.8.

The acceleration term becomes significant only at very high load rates which involve significant inertial effects, including shock waves, impact, etc. Presently we are concerned with quasi-static load situations so that the acceleration terms may be neglected.

As indicated in section 2, some modification of the constitutive law is needed to reflect work-hardening effects and to provide some correction for some of the simplifying assumptions used. By adding such a work-hardening term, $/\exp(-\phi\alpha/\alpha_0)$, and by making use of eq 3.24, eq 3.43 can be put in the following form:

$$\hat{\rho} = \frac{1}{3\alpha}\ln\left(\frac{\alpha}{\alpha-1}\right)\left\{2(S_0-C)+C\ln\left[\frac{(-\dot{\alpha}A)^2}{\alpha(\alpha-1)}\right]\right\}/\exp(-\phi\alpha/\alpha_0) \quad (3.45)$$

where ϕ and $/$ are material coefficients. This work-hardening term is of a nature consistent with the term used by St Lawrence and Bradley (1974), who noted that Gilman (1969) used a similar term for lithium fluoride crystals to account for variations in the mobile dislocation velocity. In porous snow, work hardening may be due to excessive amounts of intergranular motion that would not be present in solid polycrystalline ice. St. Lawrence and Bradley (1974) addressed this question in a more thorough manner. In addition, the model used here is rather ideal in the sense that isolation of the pores is assumed, so that the effect of one pore on another was neglected.

Simplified equation

If Y is considerably smaller than G, it can be shown that the strains incurred (and therefore α-α_0) will be quite small during the first two phases of the deformation. If such is the case, these two first phases of deformation can be neglected by representing the material as a rigid-plastic material:

$$\alpha = \alpha_0 \quad \hat{\rho} < \hat{\rho}_c$$

$$\dot{\alpha} = 0 \quad \hat{\rho} < \hat{\rho}_c \quad (3.46)$$

$$\hat{\rho} = \frac{1}{3\alpha}\ln\left(\frac{\alpha}{\alpha-1}\right)\left\{2(S_0-C)+C\ln\left[\frac{(-\dot{\alpha}A)^2}{\alpha(\alpha-1)}\right]\right\}/\exp(-\phi\frac{\alpha}{\alpha_0}) \quad > \hat{\rho}_c \quad (3.47)$$

where $\hat{\rho}_c$ is the critical stress at which the matrix material first becomes fully yielded. $\hat{\rho}_c$ is found by setting $c = b$ in eq 3.42 to yield

$$\hat{\rho}_c = \frac{/}{3\alpha_0}\ln\left(\frac{\alpha_0}{\alpha_0-1}\right)\left[2(S_0-C)+C\ln\left(\frac{(-A\dot{\alpha})^2}{(\ )-1}\right)\right]e^{-\phi}. \quad (3.48)$$

4. COMPARISON WITH EXPERIMENTAL DATA

S_0, C, and A are given in eq 2.12. The only other material constants that need to be evaluated are $/$ and ϕ, the two work-hardening coefficients. Based on data supplied by Abele and Gow (1976), these two coefficients were found to be:

$$/ = 3.07$$

$$\phi = 5.28 . \quad (4.1)$$

Eq 3.48 was adjusted to data (Abele and Gow 1976) for snow at -10°C and with an initial density of 400 kg m^{-3}.

The variation of the pressure $\hat{\rho}$ with α can then be calculated by means of eqs 2.12, 3.47 and 4.1 and compared with the data supplied by Abele and Gow (1975, 1976). The details of the experimental work are given in the reports of Abele and Gow, and the reader is referred to them for a more involved description of the experimental setup. Briefly, the tests consisted of high-rate axial compression tests in which

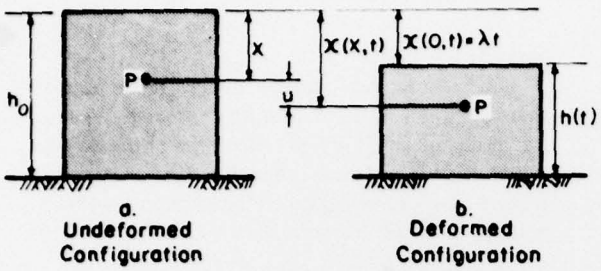

Figure 2. Description of confined compressive tests.

the specimens were constrained laterally in Teflon-lined aluminum cylinders. As a consequence, the deformation resulted in large, easily measured volumetric deformations.

Consider now the problem of the uniaxial compression of snow. If we take the x_1 direction as the axial direction and the x_2 and x_3 directions as the two lateral directions of a cylindrical specimen, the motion can be described by the equations (see Fig. 2):

$$x_1 = X_1 + \lambda t(1 - X_1/h_0)$$

$$x_2 = X_2$$

$$x_3 = X_3 \tag{4.2}$$

where X_1, X_2, and X_3 are the undeformed coordinate positions, x_1, x_2 and x_3 are the deformed coordinate positions, t is time, λ is the crosshead velocity (constant in this case), and h_0 is the initial specimen height. The Jacobian of the deformation gives

$$J = \frac{\rho_0}{\rho} = 1 - (\lambda/h_0)t \tag{4.3}$$

and therefore the density is

$$\rho = \rho_0 \left[1 - (\lambda/h_0)t\right]^{-1}. \tag{4.4}$$

The density ratio, however, is

$$\alpha = \alpha_0 \left[1 - (\lambda/h_0)t\right] \tag{4.5}$$

and its rate is

$$\dot{\alpha} = -\frac{\alpha_0 \lambda}{h_0}. \tag{4.6}$$

The constant rate tests do give a constant density ratio rate. Note, however, that the rate of change of density is not constant. For this set of experiments, $\dot{\alpha}$ was readily calculated by eq 4.6, and eq 3.47 was then utilized to find the variation of $\hat{p}$ and α for a given rate. Figure 3 shows the comparison of theory with experiment for snow at -10°C and for three initial densities. The data acquired by Abele and Gow (1975, 1976) included a variety of strain rates, since different specimen sizes and crosshead speeds were utilized. The data shown here reflect rates in the neighborhood of $\dot{\alpha} \approx 10\ s^{-1}$.

The data available from Abele and Gow (1975, 1976) measured only σ_1, the major principal stress, whereas the hydrostatic pressure $\hat{p} = 1/3\ (\sigma_1 + \sigma_2 + \sigma_3)$ was needed. Therefore, a series of experiments was run to measure lateral stress as well as axial stress so that Abele's and Gow's data could be adjusted to reflect $\hat{p}$ rather than σ_1. It was found that

$$0.6\sigma_1 < \hat{p} < 0.98\sigma_1 \tag{4.7}$$

for all the experiments run, thereby fairly well bracketing the data report by Abele and Gow (1975, 1976).

One interesting result was observed in the testing program. In tests involving "old" snow, the lateral stress was found to be about 90% of the axial stress, but for tests of "new" snow, the lateral stress was only 30-40% of the axial stress. In each case, unbonded snow (sifted within two hours of the time of testing) was used, so that the difference between the lateral stress in the old snow and that in the new snow must have been due to differences in crystal structure, primarily crystal shape. The old snow had undergone equitemperature metamorphism, and the crystals had a spherical shape. The grains, therefore, were capable of rolling and sliding relative to each other, thereby accommodating a lateral motion to produce a large lateral stress. However, new snow, with its complicated grain structure, would not allow this, thereby producing a smaller lateral stress.

As can be observed from Figure 3, the comparison between theory and experiment is quite good, with the essential characteristics of the deformation being represented by the theory.

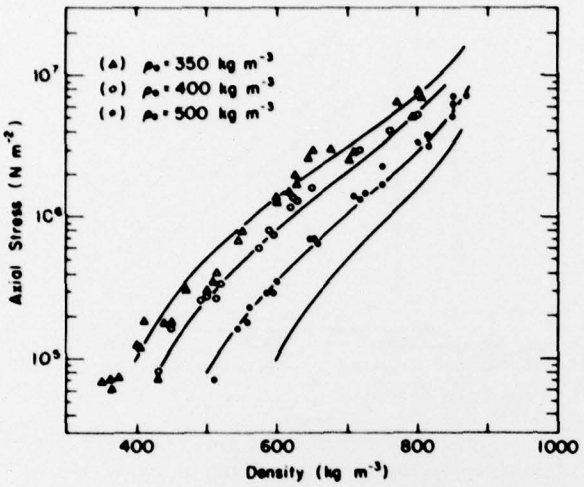

Figure 3. Comparison of theory with experimental data for snow at -10°C at three initial densities.

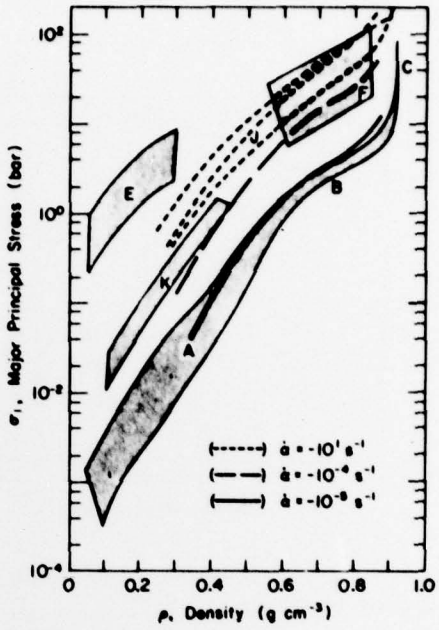

Figure 4. Comparison of theory with laboratory and field data for A *and* B*: Natural densification of snow deposits.* F, J, *and* K*: Uniaxial compression of snow.* E*: Calculated values of plane wave impact.*

Figure 4 compares theoretical pressure curves with data collected and summarized by Mellor (1974). This figure contains results of laboratory studies as well as field data relating density to gravity induced pressure. Once again the theory looks quite reasonable compared with the data. It should be remembered that some of the data shown in this figure represent uniaxial stress conditions, and that the actual hydrostatic pressures are only one-third the values shown for these data. Therefore, some of the experimental curves would move down vertically relative to the theoretical curves. However, since there is such a diverse range of load histories, temperatures, and time ranges contained in Figure 4, any meticulous adjustments would not necessarily change things that much. What can be said, though, is that eq 3.48 appears to be functionally correct for snow with initial densities exceeding 300 kg m^{-3}.

Figures 5 and 6 further describe some important properties. The deformation rate dependency is illustrated in Figure 5. For snow with an initial density of 350 kg m^{-3}, the stress response is shown as a function of density-ratio rate at three different instantaneous densities. As can be seen, a rate dependency does exist, but the importance of rate decreases as rate increases. At rates characteristic of stress waves, therefore, one might be able to assume a constant yield stress and achieve a simplified version of the constitutive law given in eq 3.48. However, for lower rates, say in the range $10^{-5} \leq |\dot{\alpha}| \leq 10$, the rate dependency is significant enough that such a simplifying procedure would not be recommended.

Figure 6 gives an indication of just how effectively snow can absorb energy during compaction. In particular, this figure shows the work required to compact snow to a terminal density of 700 kg m^{-3} for a range of initial densities and density-ratio rates. One can see immediately that initial density has a dramatic effect on work required to compress snow. Density-ratio rate is also significant but certainly much less so than initial density.

5. APPLICATION TO VEHICLE MOBILITY PROBLEMS

One obvious application of this volumetric constitutive law involves vehicle mobility in snow. Consider, for example, a vehicle travelling at a given speed along a straight path in a shallow snowpack. The vehicle is

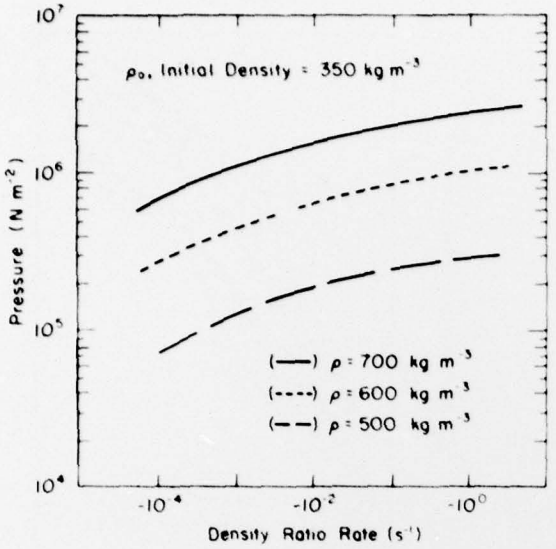

Figure 5. Variation of pressure response with rate of change of density ratio.

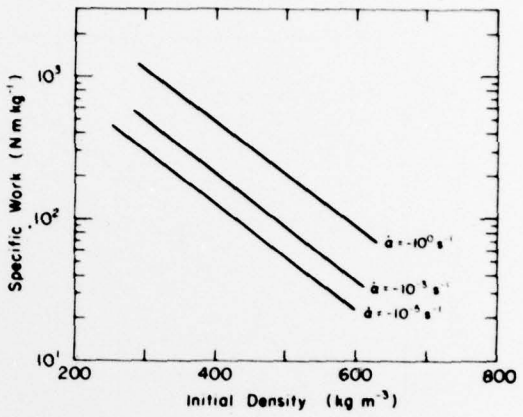

Figure 6. Effect of initial density on work required to compress snow to a density of 700 kg m^{-3}.

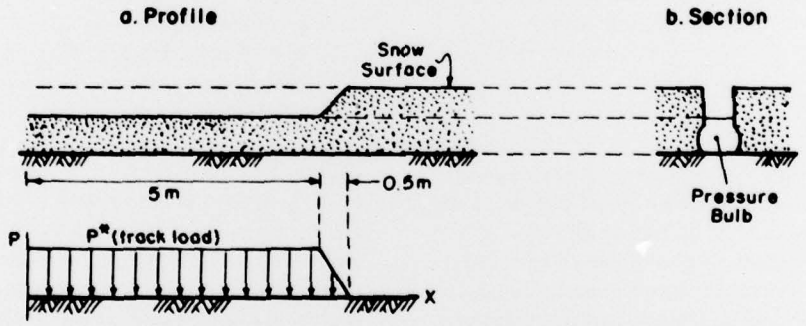

Figure 7. Profile and pressure bulb cross-section descriptions of deformation produced by tracked vehicle in snow. P = Nominal track pressure.*

assumed to be tracked. By shallow snowpack is meant a snowpack that is shallow enough so that the pressure bulb cross section reaches to the ground. Figure 7 shows a typical pressure bulb cross section. Harrison* has observed that pressure bulbs usually have a cross section that is nearly rectangular in shape. Some lateral spreading of the bulb does occur, but the added cross-sectional area is in most cases insignificant.

In situations where the vehicle is travelling at a uniform velocity and is not experiencing any significant amount of slipping, it can be reasonably assumed that the vast majority of the energy expended in traversing a snow field is associated with the energy of compacting the snow beneath the vehicle tracks. Consider a vehicle that has an idealized track loading, as depicted in Figure 7. The track pressure is assumed to build up linearly during the entry portion of the track loading. Here this is assumed to be 0.5 m, with the rest of the track having a length of 5 m. The entry length of 0.5 m is somewhat arbitrary, since this depends on the depth that the vehicle sinks into the snow.

The vehicle power associated with snow compaction is now calculated. Since the volumetric strains generated in the snowpack are large, such an analysis must use a constitutive equation valid for high strain rates and large strains. Also, any additional power requirements associated with vehicle slippage and drag would have

*Private Consultation, W.L. Harrison, CRREL.

to be added to the results which follow. The intent here is to study the manner in which snow absorbs energy through compaction.

The stress power is given by

$$\dot{W} = \frac{1}{\rho} tr(\underset{\sim}{T} \cdot \underset{\sim}{D}) \tag{5.1}$$

where $\underset{\sim}{T}$ and $\underset{\sim}{D}$ are, respectively, the Cauchy stress tensor and the rate of deformation tensor. $tr(\cdot)$ is the trace of the tensor quantity inside the parenthesis. The stress power $\dot{W}$ is simply the rate, per unit mass, at which work is being done internally by the stress tensor. For a purely viscous material under isothermal conditions, $\dot{W}$ would reduce to the rate of energy dissipation. For a viscoelastic material, the stress power would contribute to both the rate of change of strain energy and the rate of energy dissipation.

In a unidirectional deformation, the stress power associated with compaction is:

$$\dot{W} = -\frac{\hat{p}}{\rho} \frac{\partial v}{\partial x} \tag{5.2}$$

where v is the vertical particle velocity, and x is the deformed coordinate position of the particle. The continuity equation for unidirectional motion is

$$\frac{d\rho}{dt} + \rho \frac{\partial v}{\partial x} = 0. \tag{5.3}$$

Equations 5.2 and 5.3 can then be used to obtain

$$\dot{W} = -\frac{1}{\rho_m} \hat{p} \dot{\alpha}. \tag{5.4}$$

Integration results in

$$W = -\int_{t_0}^{t} \frac{\hat{p}}{\rho_m} \dot{\alpha}\, dt. \tag{5.5}$$

In the above, the pressure $\hat{p}$ is a function of time. Equation 3.48 may be inverted to yield

$$\dot{\alpha} = -e^{Q}(t, \alpha) \tag{5.6}$$

where

$$Q(t,\alpha) = \frac{1}{2}\left[F(t, \alpha) + \ln[\alpha(\alpha-1)]\right] - \ln A \tag{5.7}$$

$$F(t, \alpha) = \frac{1}{C}\left[3\alpha \hat{p}(t) e^{\phi\alpha/\alpha_o}/(J \ln(\frac{\alpha}{\alpha-1})) - 2(S_0 - C)\right]. \tag{5.8}$$

The pressure loading in the material below the track is assumed to have the form

$$\hat{p}(t) = P^* \frac{t}{t_0}\left[1 - H(t-t_0)\right] + P^* H(t-t_0) \tag{5.9}$$

where $H(t)$ is the Heaviside step function. Figure 7 shows the nature of the pressure distribution under the track. The total work done by the track to a unit mass of snow is then

$$W = \int_0^{t^*} \frac{1}{\rho_m} \hat{p}(t)\, e^{Q(t, \alpha)}\, dt \tag{5.10}$$

where t^* is the duration of time that the snow is under the track. Equations 5.7 to 5.10 can then be used to study the energetics of oversnow vehicle travel.

By substituting the assumed pressure function given by eq 5.9 into eq 5.10 and integrating over the time t^*, the actual work in compressing a unit mass of undeformed snow is found. This gives a direct measure of track efficiency for a given set of parameters such as vehicle speed, track pressure, track geometry, and snow properties.

Equation 5.2 gives the instantaneous power/unit mass of snow while the material is under the track, and this expression can vary considerably during the interval t^* of track loading. However, for the purpose of this study, the average power is more meaningful, and this is calculated by dividing the total work per unit mass W by the time period t^* required to produce this work. Therefore,

$$P = \frac{1}{t^*} \int_0^{t^*} \hat{p}(t) \frac{e^{\phi(t, \alpha)}}{\alpha} dt \tag{5.11}$$

gives the power per unit mass and is subsequently referred to as "specific power." The specific power P would have to be augmented by a factor equal to the total mass of snow under the tracks, if one wanted to find the total power requirements.

Nominally, a track length of 5 m was chosen. Track pressure was limited to 5×10^4 N m^{-2}, which admittedly is uncharacteristically low when considering military vehicles. However, such pressures are more realistic for vehicles such as snowmobiles. Initial snow densities studied range from 300 kg m^{-3} to 700 kg m^{-3}, and vehicle speeds are restricted to about 15 m s^{-1}.

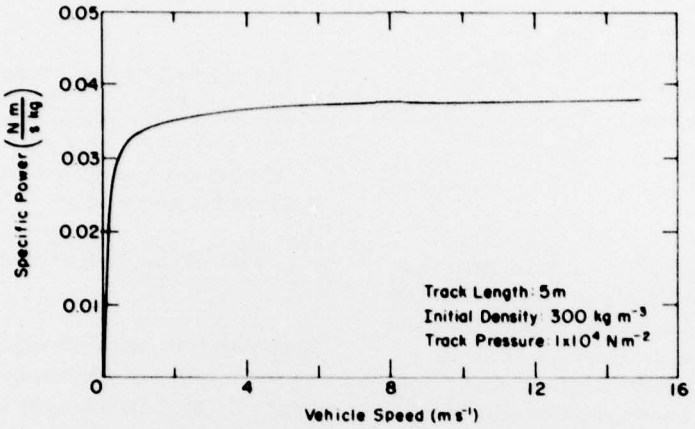

a. Track pressure $1x10^4$ N m^{-2}.

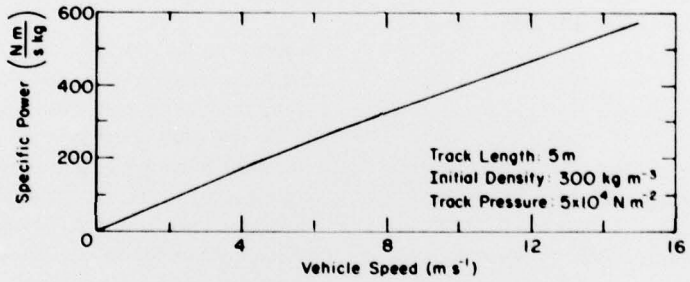

b. Track pressure of $5x10^4$ N m^{-2}.

Figure 8. Variation of specific power with vehicle speed for track pressure.

Figures 8a and b compare specific power requirements for two track loadings. A significant variation in power results when the track loading is increased from $1x10^4$ N m^{-2} to $5x10^4$ N m^{-2}. In particular, the efficiency of the lower track pressure becomes increasingly apparent at higher vehicle speeds. This is due to the decreasing amount of snow compaction that occurs while the snow is under the track as the speed increases. At the lower track loading, there appears to exist a critical speed above which little increase in efficiency is achieved with higher speeds. For the higher pressure, significant amounts of compaction continue to occur at the higher vehicle speeds. These high pressures, even at high speeds, force the vehicle a significant distance down into the snowpack, thereby expending much energy in snow compaction. At lower track pressures, the compaction becomes much less significant, and the vehicle tends to ride up on the pack, which is a much more efficient configuration.

Notice the tremendous increase in power when the track pressure is increased from $1x10^4$ N m^{-2} to $5x10^4$ N m^{-2}. Again, this can be attributed to the highly nonlinear relationship between p, α, and $\dot{\alpha}$ in the constitutive equation.

Figures 9a and b illustrate the variation of vehicle power with initial snow density. In Figure 9a, the relationship between specific power and density is illustrated for two different vehicle velocities. In Figure 9b, the same relationship is shown for three different velocities. As can readily be seen, for snow with initial densities above 300 kg m^{-3}, a track loading of $1x10^4$ N m^{-2} operates fairly efficiently. However, the same cannot be said for a track loading of $5x10^4$ N m^{-2}, where good efficiencies are not achieved for initial snow densities below 500 kg m^{-3}.

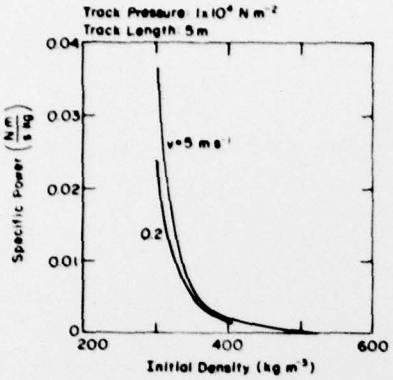

a. *Track pressure $1x10^4$ N m^{-2}.*

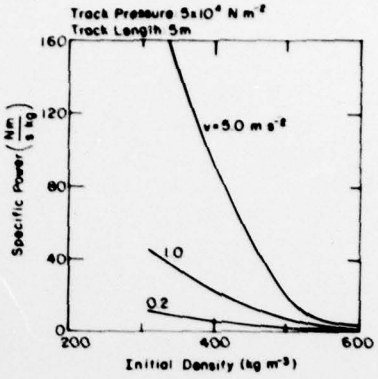

b. *Track pressure $5x10^4$ N m^{-2}.*

Figure 9. Effect of initial density on vehicle efficiency.

6. CONCLUSIONS

The volumetric constitutive equation given by eq 3.48 has been shown to correctly represent the response of snow to large monotonic compressive deformation. This equation was based on a model of pore collapse of a hollow sphere of ice, thereby giving a dynamic pore collapse relationship relating pressure to material porosity. Since work hardening was not included in the constitutive equation of the matrix material (ice), the equation had to be altered to reflect the work-hardening characteristics of snow.

The results do verify that the hydrostatic pressure is very dependent on initial porosity (or density) and only slightly dependent on rate, so that a change of four to five orders of magnitude in strain rate is required to produce an order of magnitude change in pressure. However, a small change in initial density can have a very significant effect on the pressure response of snow.

The valid range of porosity rates is apparently -10^{-5} $s^{-1} \leq \alpha \leq -10$ s^{-1} for the flow law used here for ice. The apparent valid range for initial densities includes 300 kg $m^{-3} \leq \rho_0 \leq 600$ kg m^{-3}, but at very low densities (less than 300 kg m^{-3}), it is doubtful that the physical model used to develop the constitutive law would be valid, due to a high degree of pore interconnectivity.

The results of this study indicate that the volumetric constitutive equation can be used as an engineering tool, since it does appear to give an accurate description of the response of snow to volumetric loading and is not unduly complicated in its simplified form. But some additional experimental work would be needed to adjust the equation to various snow types. However, in view of the data already acquired by Abele and Gow (1975, 1976), the amount of additional data required to do this would not be very extensive.

7. LITERATURE CITED

Abele, G. and A. Gow (1975) Compressibility characteristics of undisturbed snow. CRREL Research Report 336. AD A012113.

Abele, G. and A. Gow (1976) Compressibility characteristics of compacted snow. CRREL Report 76-21. AD A028622.

Carroll, M.M. and A.C. Holt (1972) Static and dynamic pore-collapse relations for ductile porous materials. *Journal of Applied Physics*, vol. 43, no. 4, p. 1626-1635.

Carroll, M.M. and A.C. Holt (1973) Steady waves in ductile porous solids. *Journal of Applied Physics*, vol. 44, no. 10, p. 4386-4392.

Dillon, H.B. and O.B. Andersland (1967) Deformation rates of polycrystalline ice. In *Physics of Snow and Ice* (H. Oura, ed.). International Conference on Low Temperature Science, Proceedings, vol. 1, pt. 1. Institute of Low Temperature Science, Hokkaido University, p. 313-327.

Gilman, J.J. (1969) *Micromechanics of flow in solids*. New York: McGraw-Hill Book Co., 294 p.

Hawkes, I. and M. Mellor (1972) Deformation and fracture of ice under uniaxial compression. *Journal of Glaciology*, vol. 11, no. 61, p. 103-131.

Haynes, F.D. (1976) Unpublished experimental results. CRREL.

Mellor, M. (1974) A review of basic snow mechanics. *International Symposium on Snow Mechanics, Grindelwald, Switzerland*, IAHS-AISH, publ. no. 114.

St. Lawrence, W.F. and C.C. Bradley (1974) The deformation of snow in terms of a structural mechanism. *International Symposium on Snow Mechanics, Grindelwald, Switzerland*, IAHS-AISH, publ. no. 114.